

# Importin- $\beta$ facilitates nuclear import of human GW proteins and balances cytoplasmic gene silencing protein levels

Daniel Schraivogel<sup>1</sup>, Susann G. Schindler<sup>2</sup>, Johannes Danner<sup>1</sup>, Elisabeth Kremmer<sup>3</sup>, Janina Pfaff<sup>1</sup>, Stefan Hannus<sup>4</sup>, Reinhard Depping<sup>2</sup> and Gunter Meister<sup>1,\*</sup>

<sup>1</sup>Biochemistry Center Regensburg (BZR), Laboratory for RNA Biology, University of Regensburg, Universitätsstrasse 31, 93053 Regensburg, Germany, <sup>2</sup>Institute of Physiology, Center for Structural and Cell Biology in Medicine, University of Lübeck, Ratzeburger Allee 160, 23562 Lübeck, Germany, <sup>3</sup>Institute of Molecular Immunology, Helmholtz Center Munich, German Research Center for Environmental Health (GmbH), Marchioninstraße 25, 81377 Munich, Germany and <sup>4</sup>Intana Biosciences GmbH, Lochhamerstrasse 29A, 82152 Martinsried/Planegg, Germany

Received January 07, 2015; Revised June 26, 2015; Accepted July 01, 2015

## ABSTRACT

**MicroRNAs (miRNAs) guide Argonaute (Ago) proteins to distinct target mRNAs leading to translational repression and mRNA decay. Ago proteins interact with a member of the GW protein family, referred to as TNRC6A-C in mammals, which coordinate downstream gene-silencing processes. The cytoplasmic functions of TNRC6 and Ago proteins are reasonably well established. Both protein families are found in the nucleus as well. Their detailed nuclear functions, however, remain elusive. Furthermore, it is not clear which import routes Ago and TNRC6 proteins take into the nucleus. Using different nuclear transport assays, we find that Ago as well as TNRC6 proteins shuttle between the cytoplasm and the nucleus. While import receptors might function redundantly to transport Ago2, we demonstrate that TNRC6 proteins are imported by the Importin- $\beta$  pathway. Finally, we show that nuclear localization of both Ago2 and TNRC6 proteins can depend on each other suggesting actively balanced cytoplasmic Ago – TNRC6 levels.**

## INTRODUCTION

Argonaute proteins are binding modules for small regulatory RNAs and thus essential for all small RNA-guided gene silencing pathways (1,2). Phylogenetically, Argonaute proteins are organized in three clades: the Ago clade, the Piwi clade and the worm-specific Wago (or Sago) clade. In *Caenorhabditis elegans*, 26 different Argonaute proteins exist and among them the Wago proteins fulfill very specialized functions such as binding of secondary siRNAs

or transport of siRNAs from the cytoplasm to the nucleus (3–5). The expression of Piwi proteins is restricted to the germline where they bind to Piwi interacting RNAs (piRNAs), which guide the repression of mobile genetic elements during germ cell development (6).

Ago clade members (referred to as Ago proteins hereafter) are ubiquitously expressed and interact with short interfering RNAs (siRNAs) or miRNAs (1,7). In many organisms, siRNAs can originate from exogenous or endogenous sources (endo- or exo-siRNAs) (8,9). SiRNAs guide Ago proteins to complementary sequences leading to cleavage of the target site by the bound Ago protein. Animal miRNAs, in contrast, guide Ago proteins to only partially complementary target sites mainly located in the 3' untranslated region (UTR) of mRNAs (10). Ago proteins interact with a member of the GW protein family, which are characterized by glycine-tryptophan repeats and some specific GW-pairs serve as binding platform for Ago proteins (11–17). The C-terminal half of GW proteins is referred to as the silencing domain because it coordinates all downstream steps of miRNA-guided gene silencing. First, it interacts with the poly(A) binding protein located on the poly(A) tail of the mRNA leading to inhibition of translational initiation. Second, it recruits deadenylases (e.g. the CCR4/NOT complex) to the poly(A) tail to remove it (18). To facilitate silencing, components of the CCR4/NOT complex recruit the translational repressor DDX6 to the mRNA (19,20). Finally, the shortened poly(A) tail functions as trigger for the decapping complex to remove the 5' cap of the mRNA leading to rapid degradation by 5' to 3' exoribonucleases such as Xrn1. At early stages of silencing, translational inhibition dominates whereas at later stages mRNA decay is the predominant silencing process (21–23).

Ago proteins are composed of several domains with distinct functions (24). The N domain is required for duplex

\*To whom correspondence should be addressed. Tel: +49 941 943 2847; Fax: +49 941 943 2936; Email: gunter.meister@ur.de

unwinding but also contributes to the endonucleolytic activity of Ago proteins (25–28). The PAZ domain binds the 3' end and the MID domain the 5' end of the small RNA (29–34). The PIWI domain is the endonuclease domain and harbors the catalytic center composed of DEDH (35–37). In mammals, only Ago2 possesses catalytic activity and is therefore often referred to as slicer (38,39). In addition, Ago2 seems to be the most abundant Ago protein in many mammalian cell types followed by Ago1, 3 and 4 (40,41).

Although miRNA-guided gene silencing is a cytoplasmic process, both miRNAs and Ago proteins have been found in the nucleus of mammalian somatic cells as well (5,42). They have been implicated in various nuclear processes including transcriptional silencing processes, DNA repair mechanisms or alternative splicing. It was shown that Ago proteins can be directed to promoters by transfection of promoter-specific siRNAs leading to transcriptional silencing or activation (43–45). siRNAs against nuclear target RNAs have also been widely used and nuclear RNAs can be knocked down efficiently (46,47). However, despite the numerous publications, nuclear Ago functions are still debated. This might be due to the fact that Ago proteins mainly localize to the cytoplasm in immunofluorescence experiments although minor portions are also seen in the nucleus when endogenous Ago2 is stained (46,48). In addition, Ago proteins are frequently found in nuclear fractions in biochemical fractionations. Such fractionations might often be inherently contaminated with nucleus associated cytoplasmic components and this might even be unavoidable. Not only Ago proteins but also TNRC6 proteins have been found to localize to the nucleus under specific conditions (17,49). It has been demonstrated that TNRC6A contains a nuclear localization signal (NLS) as well as a nuclear export signal (NES) and by mutation of the NES, TNRC6A remains in the nucleus where it is enriched in distinct foci demonstrating that at least TNRC6A shuttles between the nucleus and the cytoplasm (49).

Although it has been suggested that Importin-8 (Imp8) is involved in the nuclear localization of Ago2 (50,51), the requirements for nuclear transport for Ago as well as TNRC6 proteins have not been thoroughly investigated. Here, we analyzed nuclear localization and transport of Ago2 as well as the TNRC6 proteins. Using different assays, we find that Ago as well as TNRC6 proteins shuttle between the cytoplasm and the nucleus. However, we are not able to assign one specific import receptor to Ago2 and thus suggest that Importins may function redundantly in this process. Interestingly, TNRC6A is transported by the Importin- $\alpha/\beta$  family of import receptors and uses a different route into the nucleus as Ago2. Furthermore, both proteins affect nuclear import of the respective interaction partner suggesting a model in which the Ago and TNRC6 protein families balance each other's cytoplasmic levels by nuclear import.

## MATERIALS AND METHODS

### Cell lines, cell culture and generation of stable cell lines

HeLa, HEK 293T, NIH 3T3, LN-229, T98G, U-87 MG, U-2 OS, HCT116, Hep G2, HuH-7, A549, H1299, MCF7, T-47D, NCCIT, MRC-5, DU 145, GM5756, Ntera2 and Sk-Mel-28 cells were cultivated in Dulbecco's modified

Eagle's medium (DMEM) supplemented with 10% fetal bovine serum (FBS) and Penicillin/Streptomycin (P/S) antibiotics mix (all from Sigma). Arpe-19 was cultivated in DMEM/F12 (1:1) + 10% FBS + P/S (all from Sigma). DLD-1 and LNCaP were cultivated in RPMI-1640 + 10% FBS + P/S (all from Sigma). Human pulmonary artery smooth muscle cells (HPASMC) and endothelial cells (HPAEC) were purchased from Lonza and cultured in basal medium SmbM (HPASMC) and EBM-2 (HPAEC) supplemented with growth factors from SingleQuots Kit and 10% FBS (all from Lonza). Primary keratinocytes were isolated as described previously (52) and cultured in a 1:1 mixture of KSF-M and Medium 154 for keratinocytes, supplemented with epidermal growth factor and bovine pituitary extract (all from Gibco). Flp-In T-REx 293 cell line (Life Technologies) was cultivated in DMEM + 10% Tetracycline-free FBS (Clontech) + P/S + 100  $\mu$ g/ml Zeocin (Life Technologies) + 15  $\mu$ g/ml Blasticidin (Applichem).

For generation of stable inducible Flp-In T-REx 293 cell lines, cells were grown for 24 h without Zeocin and Blasticidin until transfection. Cells were cotransfected with pOG44 and pcDNA5-FRT/TO in a 9:1 ratio in 6-well format and split to one 10 cm plate one day post-transfection. Selection was started 2 days post-transfection by splitting cells into two 15 cm plates and addition of 15  $\mu$ g/ml Blasticidin and 200  $\mu$ g/ml Hygromycin B (Life Technologies). Clones were picked two weeks later and tested for Zeocin sensitivity, inducibility and expression levels. Expression was induced for 24 h with 1  $\mu$ g/ml Tetracycline (Sigma–Aldrich). Stable clones were maintained in the same medium as used for selection.

For generation of stable monoclonal HeLa cell line expressing FH-SV40NLS-Ago2, HeLa was transfected with pIRES-Flag/HA-SV40NLS-Ago2 in 6-well format. Cells were split 1 day post-transfection into one 15 cm plate and selection was started with 400  $\mu$ g/ml G418 (GE Healthcare/PAA). Clones were picked 4 weeks after transfection and tested for expression by Western Blot and immunofluorescence. Stable clones were maintained in the same medium as used for selection.

### Immunofluorescence stainings, microscopy and quantifications

For immunofluorescence stainings, cells were washed once with PBS and fixed with 4% paraformaldehyde in PBS for 10 min at 37°C. Fixation was stopped by adding PBS + 100 mM glycine for 5 min. Cells were then washed once with PBS and permeabilized with PBS + 0.1% Triton X-100 for 30 min. After washing again with PBS, cells were blocked with PBS + 0.01% Triton X-100 + 5% BSA for 30 min. First, antibody incubation was done in PBS + 0.01% Triton X-100 + 5% BSA for 1 h at room temperature. After three washing steps with PBS + 0.01% Triton X-100 + 5% BSA, secondary antibody was added for 1 h at room temperature. Cells were then washed once with PBS + 0.01% Triton X-100 + 5% BSA and trice with PBS and mounted using Prolong Gold + DAPI (Life Technologies). Confocal microscopy was done on a TCS SP8 (Leica Microsystems) equipped with acousto-optical beam splitter, 405 nm laser (for DAPI), argon laser (488 nm for Alexa 488 and GFP) and DPSS laser 561 nm

(for Alexa 555). All images were recorded using objective HC PL APO 63x/1.30 GLYC CORR CS2 and focusing to the z-section with the largest nucleus diameter. Images for quantifications were recorded with HyD SP GaAsP detectors (Leica Microsystems). Quantifications were done from tif files exported from LAS AF software. Quantification was automated using Cell Profiler v. 2.1.0 (53). We calculated nucleo-cytoplasmic ratios from mean signal values of z-sections derived from nuclear and cytoplasmic compartments. Thus, this method does not measure total nuclear or cytoplasmic protein levels in the context of the total volume of a cell. Nuclear and cytoplasmic TNRC6 foci were manually counted from 100 randomly picked cells per sample and cells were classified into cells with nuclear (>80% of TNRC6 in the nucleus), intermediate or cytoplasmic (>80% of TNRC6 in the cytoplasm) phenotype. For figure images, representative cells were selected, picture was cropped and contrast was increased to the same extent for all pictures of one panel.

### Heterokaryon assays and Leptomycin B treatments

$2 \times 10^5$  HeLa cells or stable monoclonal HeLa FH-NLS-Ago2 were plated on cover slips in 24-well plates one day before assay. Two hours before addition of NIH 3T3 cells, medium was changed to DMEM + 1% FBS + P/S + 75  $\mu$ g/ml cycloheximide (Sigma–Aldrich).  $4 \times 10^4$  cells NIH 3T3 were added to each well and co-cultured with HeLa for 2–4 h until attachment. Cells were then treated with 1 ml PBS + 50% (w/v) polyethylene glycol 1500 (Sigma–Aldrich) for 2 min at room temperature followed by five washing steps with PBS. Then, DMEM + 1% FBS + P/S + 75  $\mu$ g/ml cycloheximide was added again to cells for 4 h. Assay was stopped by adding PBS + 4% paraformaldehyde. For detection of endogenous Ago2 or FH-NLS-Ago2, cells were used for immunofluorescence staining as described above.

Leptomycin B was purchased from Cayman Chemicals as 0.1  $\mu$ g/ $\mu$ l solution in ethanol. Leptomycin B was added to cells to 10 ng/ml final concentration in standard cultivation medium. Ethanol was added to control cells without Leptomycin B. Treatments were done for 4 h and stopped by addition of PBS + 4% paraformaldehyde and subsequent immunofluorescence staining.

### In vitro transcription/translation and GST pulldown assays

GST or GST-Importins were allowed to bind to glutathione-sepharose 4B (GE Healthcare). GST-Importin pull-down assays were carried out with purified GST as a negative control as described before (54). One hundred microliters beads were pre-equilibrated in IP-buffer [20 mM HEPES pH 7.5/100 mM KOAc/112.5 mM NaCl/0.5 mM EGTA/5 mM MgOAc/250mM sucrose] at 4°C, mixed with 15  $\mu$ g GST-fusion proteins with or without His-tagged Importin- $\beta$  and incubated at 4°C for 1 h. The TNRC6A, TNRC6B, TNRC6C coding sequences – either wildtype or mutated – were transcribed and translated *in vitro* (IVTT) in the presence of [<sup>35</sup>S]-methionine (Hartmann Analytic) using TNT Coupled Reticulocyte Lysate System (Promega) according to the manufacturer's protocol from pET28a constructs. After incubation with or without purified

Ago2 or Nucleoplasmin, 10  $\mu$ l of the IVTT reaction batch were allowed to bind to the immobilized fusion proteins. After washing three times with IP-buffer, sepharose beads were dissolved in 60  $\mu$ l protein sample buffer. Twenty microliters of the reaction were separated by SDS-PAGE and visualized by Coomassie Brilliant Blue staining. For input lanes, 0.5, 5 or 10% of IVTT used for pull-downs was loaded. To detect the [<sup>35</sup>S]-labeled proteins, dried gels were autoradiographed for 16–24 h. Binding was visualized by analyzing data with a CR 35 BIO (Dürr Medical) and the Aida Image Analyser v.4.27 (Raytest).

### Antibodies

Monoclonal antibodies against the RRM domain of TNRC6A, TNRC6B and TNRC6C were generated by immunization of rats with recombinant purified RRM domains. Immunization of rats and isolation of hybridoma clones was done as described previously (55). This revealed a TNRC6B specific clone (6G3) and a clone, which recognizes all three human TNRC6 proteins (7A9). The polyclonal antibody against human Ago2 (1562) was generated by repeated injection of GST-Ago2-1–47 into rabbits. Serum was generated as described (50).

Following antibodies were used for western: rat-anti-Ago2 (monoclonal, clone 11A9, hybridoma supernatant (HS), 1:20, (48)), rabbit-anti-Ago2 (polyclonal, #1526, blood serum, 1:1.000), rat-anti-TNRC6B (monoclonal, clone 6G3, HS, 1:10), mouse-anti- $\alpha$ Tubulin (monoclonal, 1:10.000, Sigma, clone DM 1A), mouse-anti-HA (monoclonal, 1:1000, Covance, clone HA.11), mouse-anti-GFP (monoclonal, 1:1000, Roche, clones 7.1/13.1), rabbit-anti-c-Myc (1:1000, Sigma–Aldrich), rabbit-anti-Crm1 (monoclonal, 1:500, Santa Cruz Biotechnology, H-300). As secondary antibodies for Western, goat-anti-rabbit/mouse/rat IRDye 680 or 800 antibodies (Li-Cor Biosciences) were used. For Figure 7D, mouse-anti-HA (monoclonal, 1:100, Cell Signaling) and goat-anti-mouse IgG-HRP (1:2000, DAKO) were used.

Following antibodies were used for immunofluorescence stainings: rat-anti-Ago2 (monoclonal, clone 11A9, HS, 1:10), rat-anti-TNRC6B (monoclonal, clone 6G3, HS, 1:10), rat-anti-TNRC6ABC (monoclonal, clone 7A9, HS, 1:10), mouse-anti-HA (monoclonal, 1:400, Covance, clone 16B12), chicken-anti-Lsm4 (polyclonal, 1:500, Sigma–Aldrich, GW22314F), rabbit-anti-YB1 (polyclonal, 1:400, Abcam, ab12148), mouse-anti-RPA194 (monoclonal, 1:250, Santa Cruz Biotechnology, C-1), mouse-anti-RPB1 CTD (monoclonal, HS, 1:10, clone 8WG16, kindly provided by Dirk Eick), rabbit-anti-Coilin (polyclonal, 1:50, Santa Cruz Biotechnology, H-300), mouse-anti-SC35 (monoclonal, 1:500, abcam ab11862), mouse-anti-p54nrb (monoclonal, 1:200, BD Biosciences, clone 3), mouse-anti-PML (polyclonal, 1:100, Santa Cruz Biotechnology, H-238), rabbit-anti-HSF1 (monoclonal, 1:400, Cell Signaling, D3L8I), rabbit-anti-CBP80 (polyclonal, 1:100, Abcam, ab42389), rabbit-anti-CNOT7 (1:100, (56)), rabbit-anti-SKIV2L2 (polyclonal, 1:100, Novus Biologicals), rabbit-anti-Xrn2 (1:400, (57)), mouse-anti-ubiquitin (monoclonal, 1:500, Sigma, clone 6C1), mouse-anti-proteasome 20S a1,2,3,5,6,7 (monoclonal, 1:100, Enzo Life Sciences,

MCP231), mouse-anti-gH2AX (monoclonal, 1:100, Millipore, clone JBW301), rabbit-anti-53BP1 (polyclonal, 1:100, Novus Biologicals), rabbit-anti-HSF1 (polyclonal, 1:500, Cell Signalling, 4356). All primary antibodies are raised against the human proteins. As secondary antibodies, Alexa Fluor 488 or Alexa Fluor 555 coupled secondary antibodies goat-anti-mouse/rat/rabbit/chicken were used as 1:400 dilution (Life Technologies).

### Statistical analyses

Statistical analyses have been performed for the data presented in Figures 1C, E, F, H, I, J, 2B-E, 3D, 4B-C, 6B. Experiments were performed in three biological replicates. Mean values and standard error of the mean were calculated from biological replicates. Error bars display standard error of the mean. Statistical significance was calculated using two-sided Student's *t*-test for unequal sample variance. *P*-values <0.05 were considered as significant.

## RESULTS

### Nucleo-cytoplasmic distribution of human Ago2

In immunofluorescence stainings, most Ago2 is located to the cytoplasm of the cell. To find a suitable cell system to study nuclear Ago2 transport and to test whether Ago2 localization varies between cell lines, we stained endogenous Ago2 in various cell lines (Supplementary Figure S1). Most cell lines appeared to express Ago2 very similarly with the majority in the cytoplasm and a minor portion in the nucleus. However, also the minor nuclear signal is Ago2-specific since Ago2 knock down leads not only to a reduction of the cytoplasmic but also the nuclear pool ((48) and see below). Of note, Ago2 is also found in the nuclear fraction of HeLa cell lysates (see Figure 3E).

To further solidify that Ago2 is indeed found in the nucleus, we applied a modified heterokaryon assay, in which mouse NIH 3T3 cells are fused with HeLa cells and human Ago2 redistribution into the mouse nucleus is investigated (Figure 1A). The shuttling protein hnRNPA1 served as positive control and was detectable in the mouse nucleus after cell fusion (Figure 1B, top). HnRNPC was used as negative control and remained solely in the human nucleus (Figure 1B, bottom). When endogenous Ago2 was analyzed, we found that human Ago2 levels increased slightly but clearly measurable over background signal in the mouse nucleus (Figure 1C) indicating that human Ago2 reaches the mouse nucleus. Similar results were obtained when eGFP-tagged Ago2 was analyzed (Supplementary Figure S1D). Whether it shuttles from the human nucleus or whether it is redistributed from the cytoplasm is unclear. To test this further, we fused Ago2 to the strong SV40 NLS and forced it into the nucleus. When these cells were fused with NIH 3T3 cells, SV40 NLS-Ago2 still appeared in the mouse nucleus although cycloheximide has been added and synthesis of new proteins can be excluded (Figure 1D, upper panel). Nevertheless, the nuclear pool found in mouse nuclei after fusion can still originate from the small cytoplasmic SV40 NLS-Ago2 pool (Figure 1E). However, when cells were treated with leptomycin B (LMB), which is an inhibitor of Crm1-mediated nuclear export (58), before fusion, significantly

less nuclear SV40 NLS-Ago2 was found in the mouse nucleus (Figure 1D, lower panel and 1F for quantification) demonstrating that NLS-Ago2 indeed shuttles from the human to the mouse nucleus. To further solidify the observed nucleo-cytoplasmic shuttling activity of Ago2, we treated HeLa (Figure 1G and H and Supplementary Figure S2) and another cell line, Sk-Mel-28, with LMB (Figure 1H). Sk-Mel-28 is a melanoma-derived cell line with high levels of nuclear Ago2 (Supplementary Figure S1). Under these conditions, the nuclear Ago2 pool increased significantly, suggesting that endogenous Ago2 shuttles between the nucleus and the cytoplasm but is mainly localized to the cytoplasm under steady-state conditions (Figure 1G right panel and 1H for quantification). RNA interference (RNAi) against Ago2 decreased both the cytoplasmic as well as the nuclear signal showing that the observed signal is indeed endogenous Ago2 and not caused by antibody cross reactivity (Figure 1I and J). Consistent with these observations, Crm1 knock down increased nuclear Ago2 staining (Supplementary Figure S3A). Thus, our data show that human Ago2 is able to enter the nucleus and most likely shuttles between the nucleus and the cytoplasm with only a minor portion being found in the nucleus under steady state conditions.

### Nuclear transport of human Ago2

It has been suggested that Imp8 is involved in the nuclear transport of Ago2 (50,51). To test the requirement of import receptors for nuclear Ago2 localization, we established a nuclear RNAi activity assay, in which the nuclear RNA 7SK is knocked down (Figure 2A). 7SK is part of a nuclear ribonucleoprotein particle involved in the regulation of transcriptional elongation (59). To validate this system, we depleted Ago1–4 (Figure 2B) and analyzed 7SK knock down efficiency (Figure 2C). Indeed, only when Ago2 is depleted, the 7SK knock down is reduced demonstrating that the measured effects are Ago2-dependent and the assay is suitable for the analysis of Ago2 import routes. Subsequently, we knocked down Impβ, Imp3–5, Imp7–9, Imp11–13 and transportin-1 (Tnp1) (Figure 2D for knock down efficiencies). However, none of the tested knock down conditions resulted in a reproducible change in 7SK knock down efficiency (Figure 2E). Thus, we conclude that at least in this nuclear RNAi assay, knock down of a single import receptor is not sufficient to prevent nuclear Ago transport. It is conceivable that several import receptors function redundantly in transporting Ago proteins into the nucleus as has been reported for human Dicer, for example (60).

### Nuclear localization of the human TNRC6 proteins

It has been demonstrated that TNRC6 proteins can localize to the nucleus under specific conditions (17,49). TNRC6A, for example, contains an NES and when mutated, over expressed and tagged TNRC6A accumulates in nuclear foci of unknown origin (49). To analyze TNRC6 protein transport in molecular detail, we expressed FLAG/HA-tagged (FH)-TNRC6A-C and treated the cells with LMB for Crm1-dependent nuclear export inhibition (Figure 3A). We observe that all three TNRC6 proteins accumulate in nuclear foci upon LMB treatment. This is a clear and widespread effect as shown by quantification of nuclear and cytoplasmic

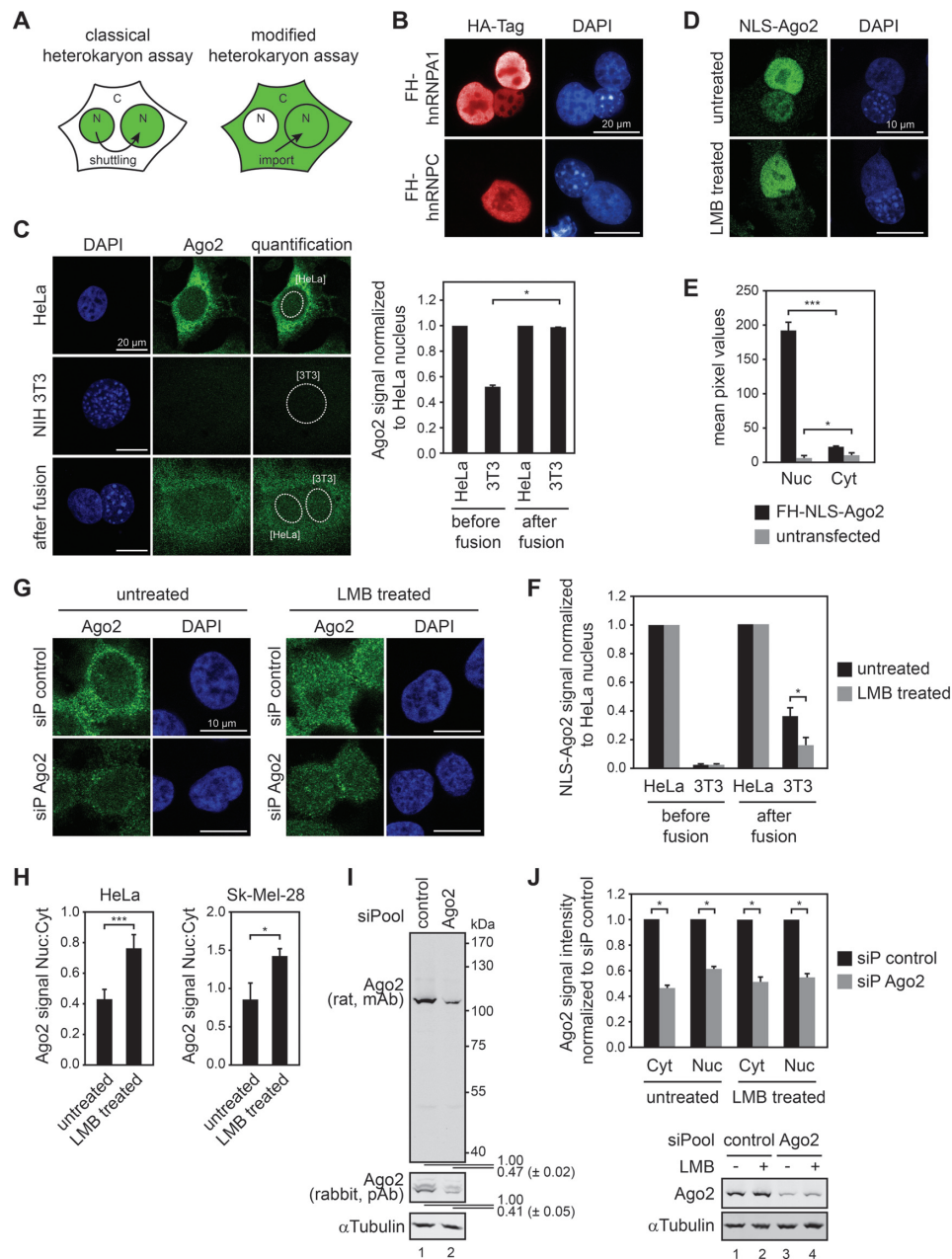


**Figure 1.** Ago2 is imported into the nucleus of human cells and shuttles between the nucleus and the cytoplasm. (A) Classical and modified heterokaryon assays. (B) HeLa cells transfected with FH-hnRNPA1 and FH-hnRNPC were fused to mouse NIH 3T3 cells. After fusion, FH-hnRNPA1 appears in the mouse nucleus characterized by intense DAPI staining from densely packed pericentromeric heterochromatin. FH-hnRNPC does not shuttle and remains in the human nucleus. (C) HeLa cells treated with cycloheximide were fused to mouse NIH 3T3 cells and endogenous Ago2 was detected with a monoclonal anti-Ago2 antibody. Microscopy shows Ago2 staining in unfused HeLa cells (upper panels) and no signal in unfused NIH 3T3 cells (middle panels). After fusion, Ago2 is detected in heterokaryon cytoplasm and both human and mouse nuclei (lower panels). Diagram on the right shows quantification of Ago2 signal from human and mouse nuclei before and after cell fusion with data normalized to human nucleus. (D) Heterokaryon assays were performed with HeLa cells stably transfected with FH-SV40NLS-Ago2 with or without Leptomycin B treatment. Ago2 was detected by anti-HA antibody staining. (E) Nuclear and cytoplasmic levels of FH-NLS-Ago2, which was detected with an anti-HA antibody and quantified from nucleus and cytoplasm before fusion with mouse NIH 3T3. (F) Quantification of Ago2 signal from human and mouse nuclei before and after fusion of untreated or Leptomycin B treated cells shown in Figure 1D. Quantification was performed as described in Figure 1C. (G) HeLa cells were untreated or treated with Leptomycin B and endogenous Ago2 was detected with anti-Ago2 antibody. Upper panels show cells transfected with a control siPool, lower panels show cells transfected with a siPool against Ago2. (H) Signal quantification from untreated or Leptomycin B treated HeLa (left panel) and Sk-Mel-28 (right panel) cells. Ago2 signal intensity was detected in the nucleus and cytoplasm and nucleus-to-cytoplasm ratio was calculated. (I) Ago2 protein levels were analyzed upon knockdown of Ago2 or transfection of a control siPool with two different antibodies. Western Blot with anti- $\alpha$ Tubulin antibody was used as loading control. Signal quantifications of knockdown versus control were normalized to  $\alpha$ Tubulin and shown with standard error of the mean. (J) Nuclear and cytoplasmic Ago2 pools are equally reduced by RNAi against Ago2. Ago2 signal was quantified from nucleus and cytoplasm in untreated or Leptomycin B treated cells upon knockdown of Ago2 or transfection of a control siPool. Signals were normalized to control siPool. Western blot below shows Ago2 expression in untreated (lanes 1, 3) or Leptomycin B treated (2, 4) cells after transfection of a control siPool (1, 2) or Ago2 (3, 4) siPool.  $\alpha$ Tubulin was detected loading control. Error bars represent standard error of the mean (SEM). \* $P$  < 0.05; \*\*\* $P$  < 0.0005.

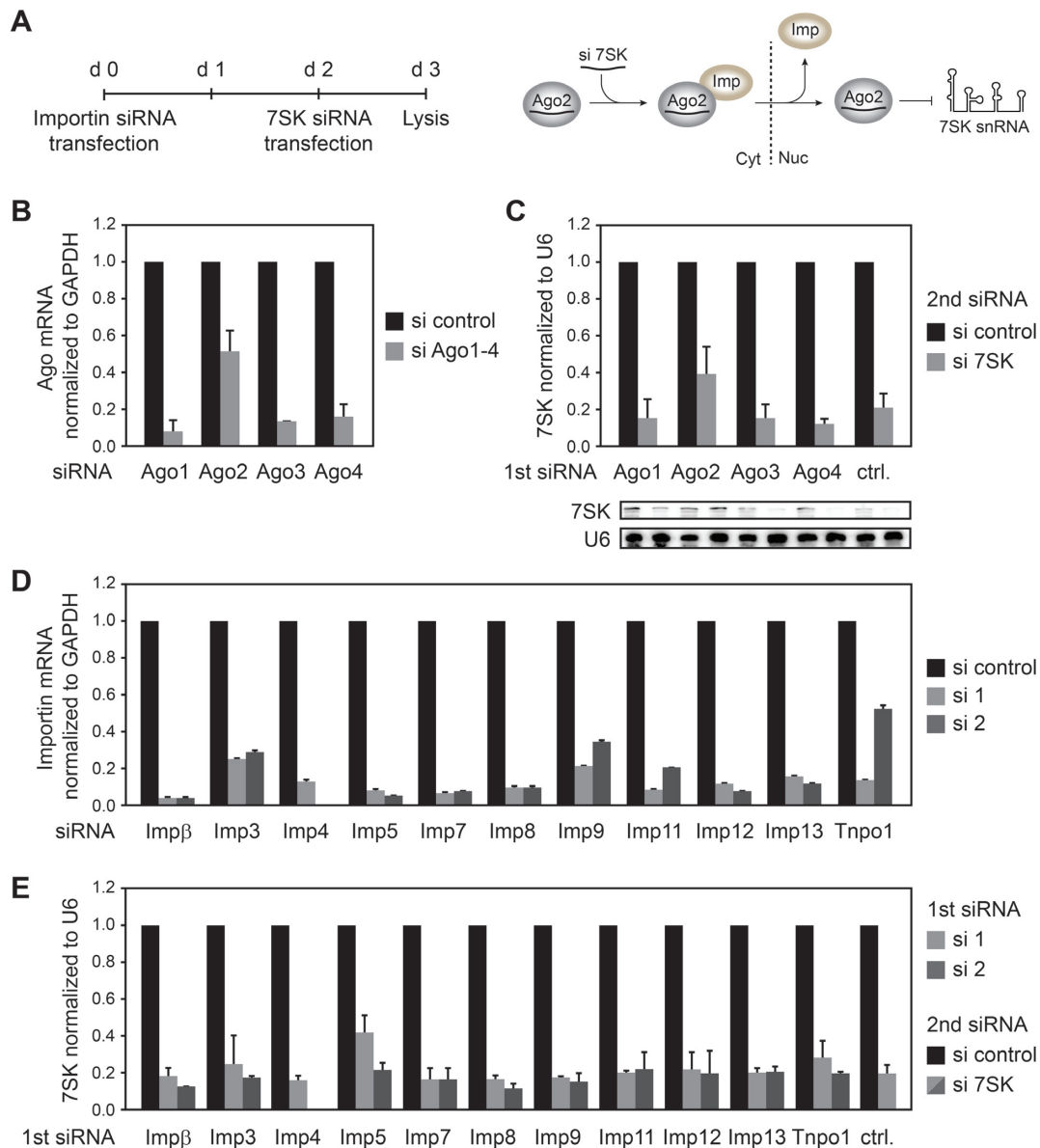


**Figure 2.** Ago2 nuclear import is presumably mediated by several redundant import receptors. (A) Schematic representation of the experimental procedure to measure nuclear Ago2 activity upon Importin knock down. Nuclear Ago2 activity was determined from knock down efficiency of the nuclear 7SK snRNA. (B) Knock down efficiency of Ago1–4 was determined by quantitative real-time PCR. Data were normalized to GAPDH mRNA and control siRNA transfected sample. (C) Knock down of human Ago1–4 followed by knock down of 7SK snRNA. Lower panels show Northern Blots probed for 7SK and U6 snRNAs. 7SK signal was normalized to U6 in the corresponding sample and control siRNA transfected sample (upper panel). (D) An Importin siRNA library targeting each human Importin, except for Imp $\alpha$ , was generated and validated for knock down efficiency by quantitative real-time PCR. Except for Imp4, two siRNAs (si1, si2) were generated for each Importin. Data were analyzed as described in Figure 2B. (E) The Importin siRNA library was used to knock down human Importins followed by analysis of 7SK knock down efficiency as described in (A). Data were analyzed as described in (B).

foci (Figure 3A, panel below left). All three full-length proteins were readily detectable in Western blots (Figure 3A, below right). Co-staining with marker proteins for diverse nuclear compartments, complexes and other structures did not show any co-localization with TNRC6A. Only Ago2 is occasionally found in these nuclear TNRC6A bodies (Supplementary Figure S4). Over expression of proteins can sometimes cause unspecific localization. Thus, we generated monoclonal antibodies against TNRC6B in order to analyze endogenous protein. In biochemical fractions of

nuclear and cytoplasmic extracts, TNRC6B was found in both compartments (Figure 3B). Next, we performed LMB treatment experiments as described above (Figure 3C and D). Strikingly, LMB treatment caused a nuclear accumulation of endogenous TNRC6B although not in such discrete foci as observed with over expression of TNRC6B, a phenomenon that is also observed for cytoplasmic P-bodies when Ago or TNRC6 proteins are over expressed (61). Crm1 knock down resulted in similar effects (Supplementary Figure S3B). The signal is highly specific to TNRC6B

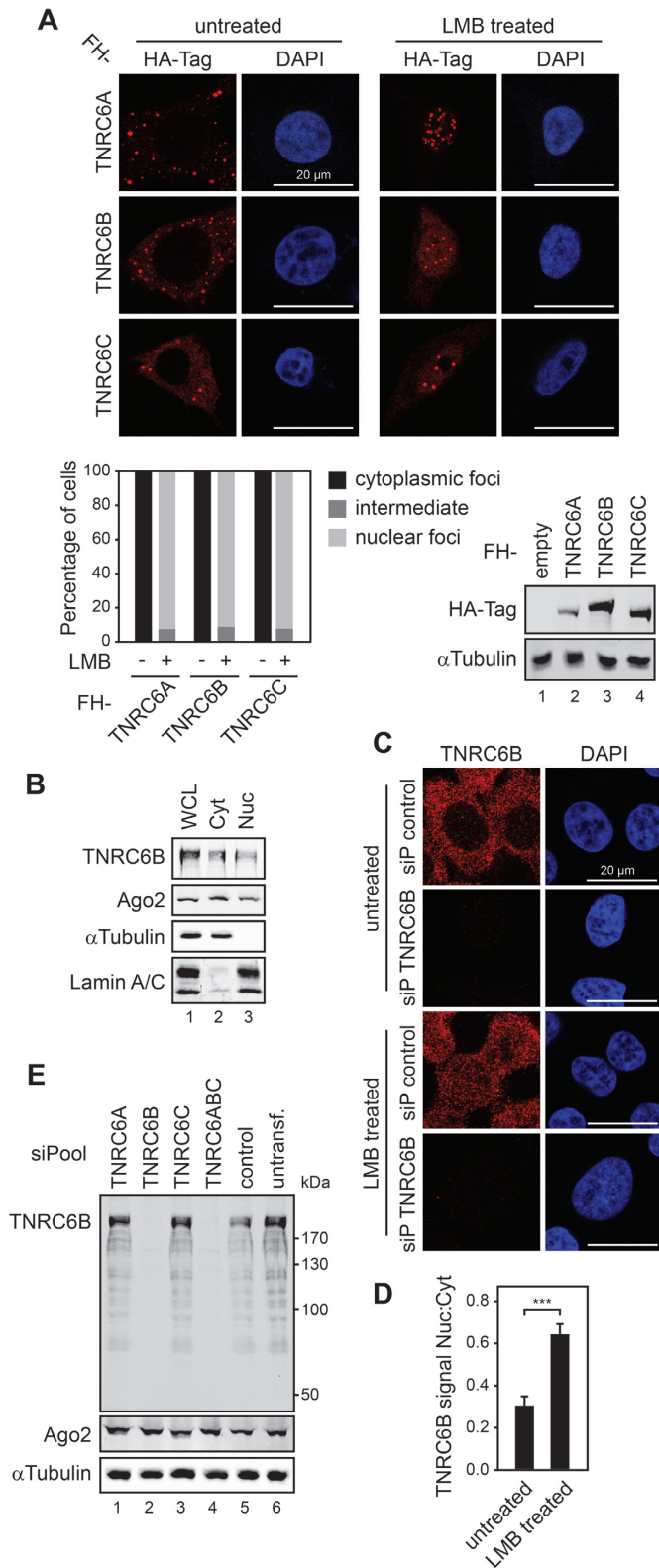


**Figure 3.** Human TNRC6 proteins shuttle between the nucleus and cytoplasm. (A) HeLa cells transfected with FH-TNRC6A, FH-TNRC6B or FH-TNRC6C were left untreated or treated with Leptomycin B and TNRC6 proteins were detected with anti-HA antibodies. Diagram below shows the percentage of cells with cytoplasmic foci, nuclear foci or cells with foci in both compartments (intermediate) with or without

since knock down using a siPool (62) against TNRC6B (Figure 3E for knock down validation) resulted in a complete loss of the signal (Figure 3C and D). Thus, we conclude that all three TNRC6 proteins shuttle between the nucleus and the cytoplasm and their export route is Crm1-dependent.

### TNRC6 protein import requires Importin-β

To assess how TNRC6 proteins are imported into the nucleus, we knocked down a series of import receptors and analyzed TNRC6A nuclear localization (Figure 4). As a test system for nuclear import of TNRC6 proteins, we utilized a TNRC6A variant containing a mutated NES (TNRC6A NES-mut), which is trapped in the nucleus (49). Two days after transfection of the individual siRNAs (see Figure 2), TNRC6A NES-mut was induced and its localization analyzed (Figure 4A and Supplementary Figure S5). While knock down of most import receptors did not lead to a cytoplasmic retention of TNRC6A NES-mut, depletion of Impβ caused a predominant cytoplasmic localization of over expressed TNRC6A NES-mut suggesting nuclear import by Impβ (Figure 4A, right panel for quantification). To further verify these observations, we analyzed localization of endogenous TNRC6B upon LMB treatment (Figure 4B). Strikingly, endogenous TNRC6B trapped in the nucleus after LMB treatment, but not when Impβ was depleted. Taken together, our results demonstrate that TNRC6 proteins enter the nucleus in an Impβ-dependent pathway. Although we did not observe effects of Impβ on Ago localization in our previous experiments (Figure 2), we asked whether at least a small fraction of Ago2 could be co-transported together with TNRC6B. Upon LMB treatment, the nuclear Ago2 signal increased (Figure 4C). However, unlike TNRC6B, Impβ knock down had no effect on nuclear Ago2 accumulation under these conditions indicating that both gene-silencing components are imported into the nucleus by different transport routes.

### TNRC6 proteins interact with Impβ

In the canonical Impβ pathway, Impα binds the NLS of cargo proteins and recruits Impβ, which facilitates nuclear import whereas non-canonical import by Impβ can be mediated by direct interaction with cargo proteins (63,64). To

Leptomycin B treatment. Western Blot shows expression of FH-tagged TNRC6A-C (lanes 2–4) or empty plasmid (lane 1) with αTubulin as loading control. (B) Whole cell lysate (WCL, lane 1), cytoplasmic (Cyt, lane 2) and nuclear (Nuc, lane 3) extracts were prepared from HeLa cells and endogenous TNRC6B or Ago2 were detected by Western Blotting. αTubulin and Lamin A/C were detected as cytoplasmic and nuclear controls. (C, D) Endogenous TNRC6B was detected with a monoclonal anti-TNRC6B antibody in control siPool or TNRC6B siPool transfected cells with (upper panels) or without (lower panels) Leptomycin B treatment. TNRC6B signal intensity was detected in the nucleus and cytoplasm and nucleus-to-cytoplasm ratio is shown in (D). (E) TNRC6B and Ago2 protein levels were detected with monoclonal antibodies upon knock down of TNRC6A, TNRC6B, TNRC6C or all three TNRC6 proteins (lanes 1–4). Control siPool transfected cells (lane 5) or untransfected cells (lane 6, untransf.) were used as control. Western Blot with an anti-αTubulin antibody was used as loading control. Error bars represent standard error of the mean (SEM). \*\*\**P* < 0.0005.

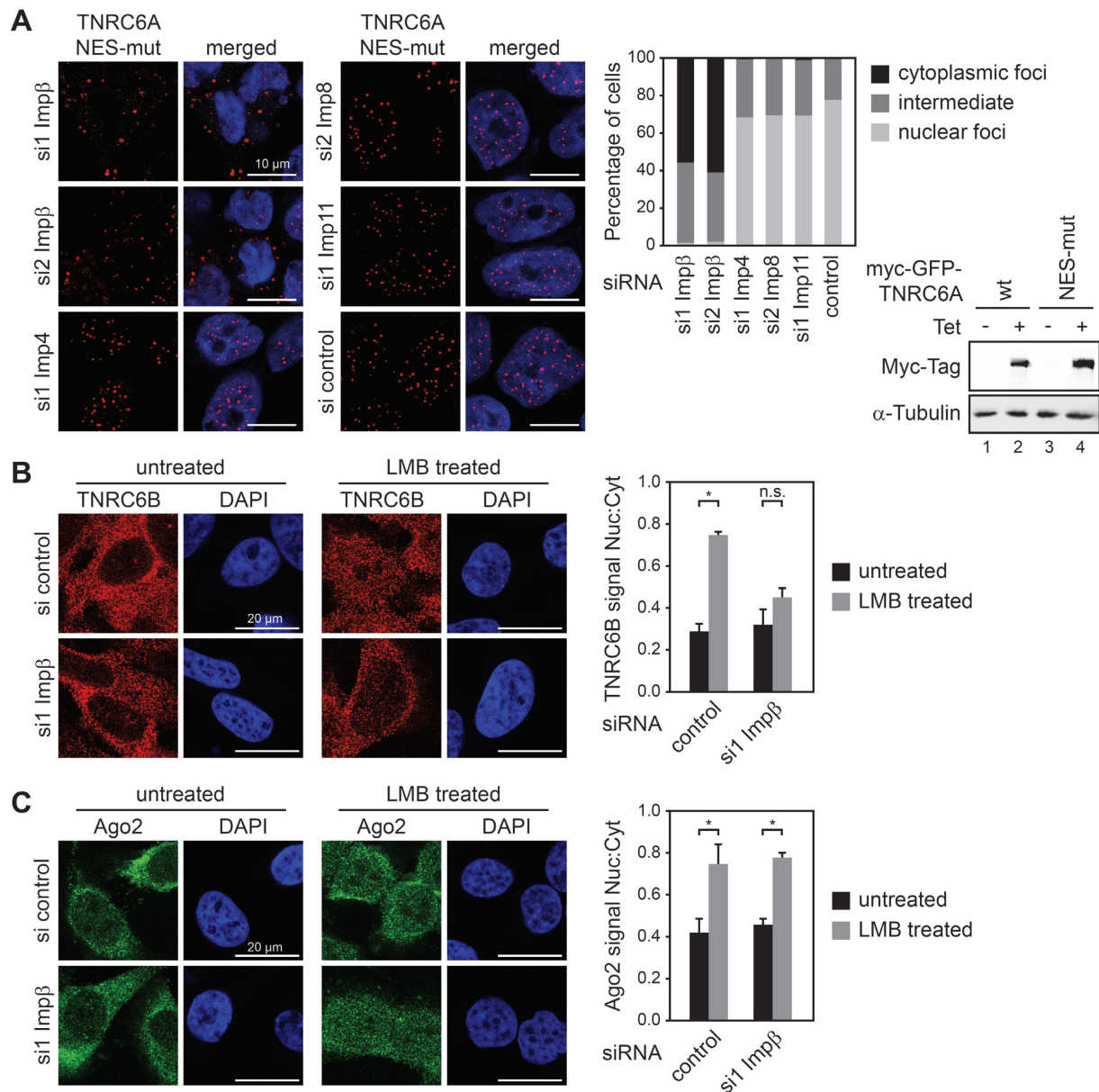


**Figure 4.** Nuclear import of TNRC6 proteins is facilitated by Importin- $\beta$ . (A) HEK 293T cells with stably integrated and inducible myc-GFP-TNRC6A NES-mut were transfected with Importin siRNAs. Expression of nuclear-trapped myc-GFP-TNRC6A NES-mut was induced 1 day before analysis. Diagram on the right shows percentage of cells with cytoplasmic or nuclear GFP foci and cells with foci in both compartments (intermediate). Western blot shows expression of myc-GFP-TNRC6A wildtype (wt, lane 1 and 2) and NES-mut (lanes 3 and 4) with and without induction by tetracycline (Tet, lanes 2 and 4) as detected using anti-Myc-Tag antibody.  $\alpha$ Tubulin was used as loading control. (B) Endogenous TNRC6B was detected in untreated or Leptomycin B treated HeLa cells upon knockdown of Imp $\beta$  or transfection of a control siRNA. Diagram shows quantification of TNRC6B signal from untreated or Leptomycin B-treated cells with or without knockdown of Imp $\beta$ . Nucleus-to-cytoplasm ratio was calculated from nuclear and cytoplasmic TNRC6B signals. (C) Endogenous Ago2 was detected in HeLa cells and quantified as described in (B). Error bars represent standard error of the mean (SEM). \* $P < 0.05$ . n.s.,  $P > 0.05$ .

test Imp $\alpha$ / $\beta$ -TNRC6 interactions, we performed *in vitro* binding assays (Figure 5A-D). Since Imp $\beta$  can also affect Imp $\alpha$ 's binding affinity to cargo proteins (65,66), binding of both proteins was analyzed. Different isoforms of GST-Imp $\alpha$  ( $\alpha 1$ ,  $\alpha 3$ ,  $\alpha 4$ ,  $\alpha 5$  and  $\alpha 7$ ) as well as GST-Imp $\beta$  were immobilized and incubated with radiolabeled TNRC6A. Either His-Imp $\beta$  was added to the Imp $\alpha$  samples (Figure 5A) or Imp $\alpha$  was analyzed alone (Supplementary Figure S6). Indeed, moderate binding of TNRC6A was observed for

the Imp $\alpha$  isoforms in the presence Imp $\beta$ . In the absence, however, binding was reduced (Supplementary Figure S6). In addition, TNRC6A binding to Imp $\beta$  alone was readily detectable indicating Imp $\alpha$ -independent Imp $\beta$  contacts to TNRC6A (Figure 5A, lane 6). Since our experiments are not quantitative, conclusions regarding binding affinities are not possible. To elucidate this observation further, we performed binding experiments with TNRC6A containing mutations in a recently suggested NLS (49) (Figure 5B).

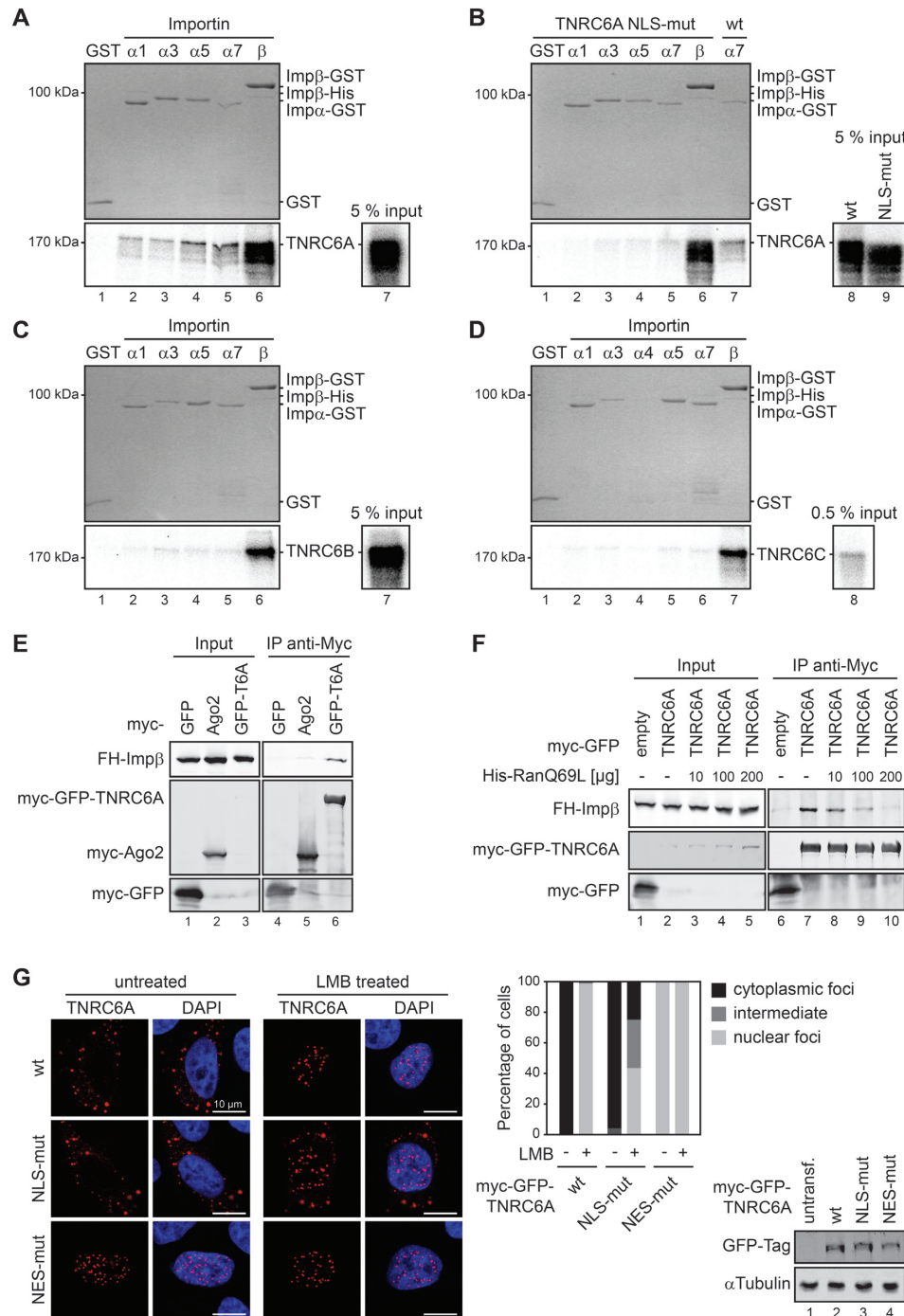


**Figure 5.** Importin- $\alpha$  and Importin- $\beta$  interact with TNRC6 proteins. (A) *In vitro* transcribed and translated TNRC6A was incubated with recombinant GST alone (lane 1), GST-tagged Imp $\alpha$ -family members and Imp $\beta$ -His (lanes 2–5) or Imp $\beta$ -GST alone (lane 6) followed by GST-pulldown. TNRC6A was detected by autoradiography, recombinant proteins by Coomassie staining. Lane 7 shows input of TNRC6A. (B) *In vitro* transcribed and translated TNRC6A NLS-mut (lanes 1–6) or TNRC6A (lane 7) was incubated with GST alone or the indicated Importins and pulled down as described in (A). Lanes 8 and 9 show inputs of TNRC6A and TNRC6A NLS-mut. (C, D) *In vitro* transcribed and translated TNRC6B (C) and TNRC6C (D) were incubated with GST alone (lane 1) or the indicated Importins (lanes 2–6 in C and 2–7 in D) and pulled down as described in (A). Lane 7 in (C) and 8 in (D) show inputs of TNRC6B or TNRC6C. All autoradiographs in (A–D) have been exposed simultaneously. (E) FH-Importin has been cotransfected with myc-GFP (lane 1 and 4) or myc-Ago2 (lanes 2 and 5) in HEK 293T cells or transfected into HEK 293T with stable inducible myc-GFP-TNRC6A cultivated in the presence of Tetracycline (lanes 3 and 6). Myc-tagged proteins were immunoprecipitated from cytoplasmic extracts with anti-Myc antibody. Immunoprecipitations were analyzed with anti-HA and anti-Myc antibodies. (F) Immunoprecipitations have been performed as described in (E), excluding myc-Ago2, in the absence (lanes 1, 2, 6 and 7) or presence of increasing amounts of recombinant His-tagged RanQ96L, preincubated with GTP (lanes 3–5 and 8–10). (G) HeLa cells were transfected with myc-GFP-TNRC6A, NLS-mut or NES-mut followed by treatment with Leptomycin B or control treatment. Diagram shows percentage of cells with cytoplasmic or nuclear GFP foci or foci in both compartments (intermediate) with or without Leptomycin B treatment. Western Blot shows expression of myc-GFP-TNRC6A wildtype (wt, lane 2), NLS-mut (lane 3) and NES-mut (lane 4) as detected using anti-GFP antibody. Untransfected (untransf.) cells were loaded as control and  $\alpha$ Tubulin was detected as loading control.

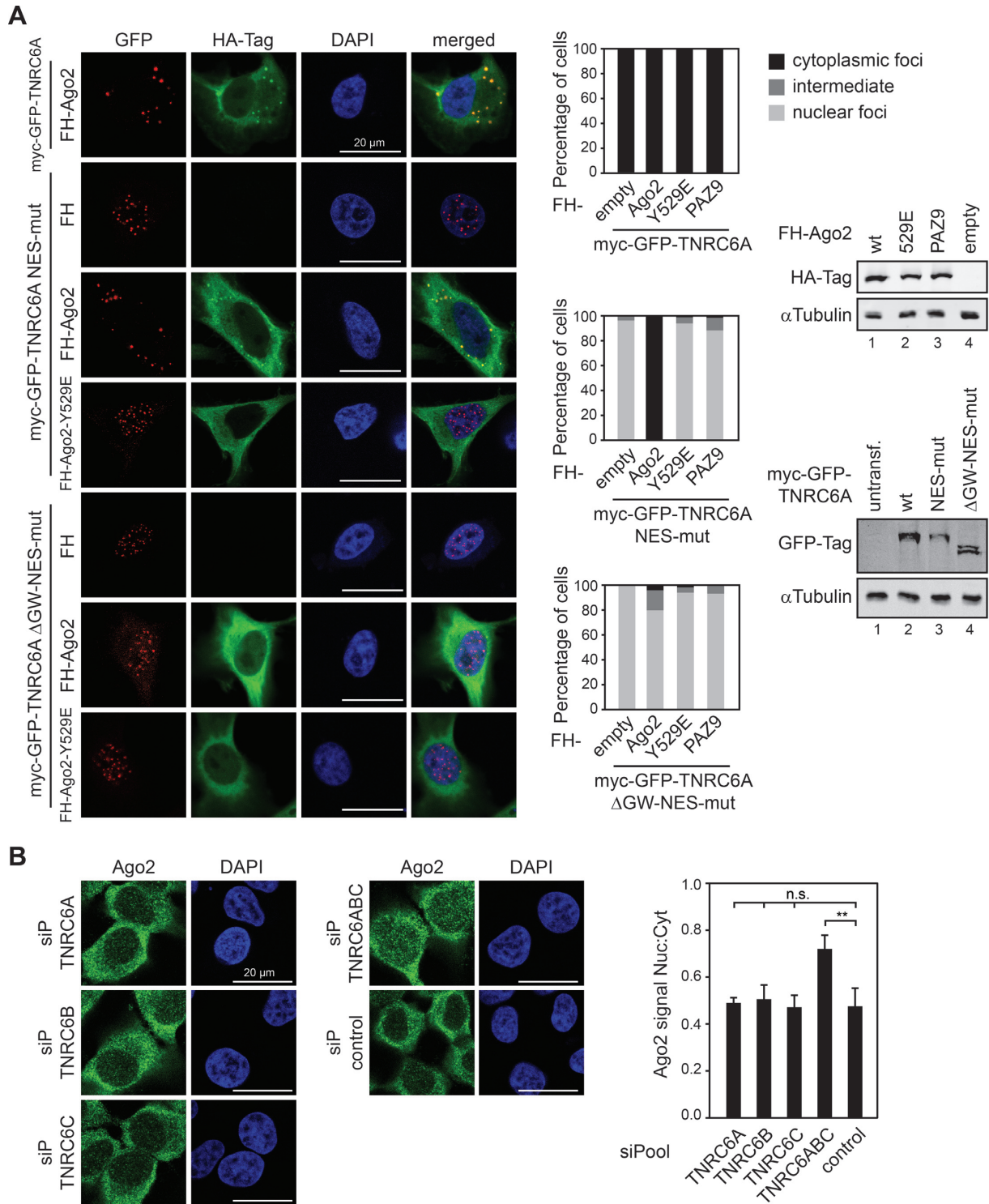


**Figure 6.** Reciprocal cytoplasmic retention of TNRC6 and Ago2. (A) HeLa cells were cotransfected with myc-GFP-TNRC6A, NES-mut or  $\Delta$ GW-NES-mut and FH-Ago2, Y529E, PAZ9 or empty plasmid (FH). TNRC6A and its mutants were detected by GFP signal (shown here in red), Ago2 and its mutants with anti-HA antibody staining (shown in green). Diagrams on the right show percentage of cells with cytoplasmic or nuclear GFP foci or foci in both compartments (intermediate). Ago2 PAZ9 is shown as diagram only. Western blots on the right show expression of FH-Ago2 and its mutants (upper Blot) or myc-GFP-TNRC6A and its mutants (lower Blot).  $\alpha$ Tubulin was detected as loading control. (B) TNRC6A, TNRC6B and TNRC6C were knocked down each on its own or simultaneously in HeLa cells and endogenous Ago2 was detected by anti-Ago2 antibody staining. A control siPool served as negative control. Diagram on the right shows nucleus-to-cytoplasmic ratio of Ago2 by quantification of nuclear and cytoplasmic signals. Error bars represent standard error of the mean (SEM). \*\* $P < 0.005$ .

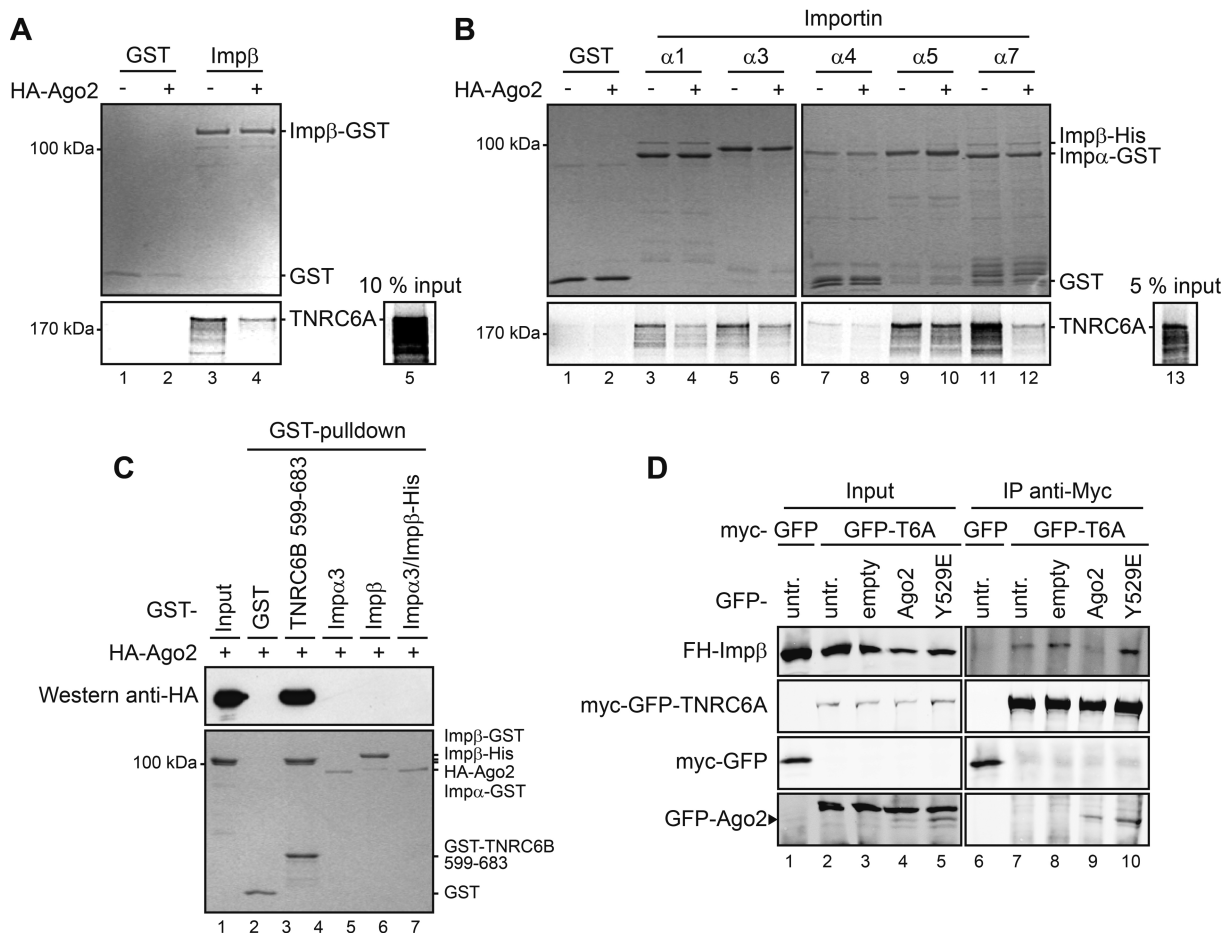


**Figure 7.** Ago2 blocks binding of Importin- $\alpha$  and Importin- $\beta$  to TNRC6A. **(A)** *In vitro* transcribed and translated TNRC6A was incubated with recombinant GST (lanes 1 and 2) or Imp $\beta$ -GST (lanes 3 and 4). Additionally, recombinant HA-Ago2 was added when indicated (even lanes). After GST-pulldown, TNRC6A was detected by autoradiography, recombinant proteins by Coomassie staining. Lane 5 shows TNRC6A input. **(B)** *In vitro* transcribed and translated TNRC6A was incubated with recombinant GST (lanes 1 and 2) or GST-tagged Imp $\alpha$ -family members and Imp $\beta$ -His (lanes 3–12). Recombinant HA-Ago2 was added when indicated (even lanes). Experiments were analyzed as described in (A). Lane 13 shows TNRC6A input. **(C)** Recombinant GST (lane 2), GST-tagged TNRC6B 599–683 (lane 3), Imp $\alpha$ 3 (lane 4), Imp $\beta$  (lane 5) and Imp $\alpha$ 3 + Imp $\beta$ -His (lane 6) were incubated with HA-tagged recombinant Ago2. After GST-pulldown, Ago2 was detected in input (lane 1) and pulldowns (lanes 2 to 7) by anti-HA antibody. Proteins in input and pulldowns were additionally detected by Coomassie staining. **(D)** Coimmunoprecipitations with anti-Myc antibody were performed from HEK 293T cells coexpressing Flag/HA-tagged Imp $\beta$  and myc-GFP (lane 1 and 6) or myc-GFP-TNRC6A (lanes 2 and 7). Additionally, GFP (lanes 3 and 8), GFP-Ago2 (lanes 4 and 9) or GFP-Ago2 Y529E (lanes 5 and 10) were coexpressed. Immunoprecipitations were analyzed with anti-HA (FH-Imp $\beta$ ), anti-Myc (myc-GFP-TNRC6A and myc-GFP) and anti-GFP antibodies (GFP-Ago2 or GFP-Ago2 Y529E).

Binding of Imp $\alpha$  to this mutant appeared to be weaker. Binding to Imp $\beta$ , however, remained unaffected. Our data suggest that the reported NLS contributes to nuclear transport, potentially via Imp $\alpha$ , but is not sufficient and additional TNRC6A elements are required. We next investigated binding of the import proteins to TNRC6B and C (Figure 5C and D). Similarly to TNRC6A, Imp $\beta$  efficiently bound TNRC6B and C. In contrast, binding to the Imp $\alpha$  isoforms was not observed (Figure 5C and D) consistent with the finding that classical Imp $\alpha$ -dependent NLS were not found in TNRC6B and C (49).

To confirm our *in vitro* binding results, we performed co-immunoprecipitation experiments (Figure 5E and F). FH-Imp $\beta$  was co-transfected with myc-Ago2 or myc-GFP as control into HEK 293 cells. For better expression levels, myc-GFP-TNRC6A was stably transfected. Indeed, FH-Imp $\beta$  was co-immunoprecipitated with anti-myc-GFP-

TNRC6A but not with myc-Ago2 or the control (Figure 5E). Furthermore, incubation of the immunoprecipitates with RanQ69L, a Ran mutant that destabilizes Importin – cargo interactions (67), interrupted with TNRC6A binding to Imp $\beta$  (Figure 5F). Our binding experiments therefore suggest that Imp $\beta$  interacts with TNRC6A in a Ran-dependent manner.

To further validate the reported NLS, we performed LMB treatment experiments (Figure 5G). While wild type (wt) TNRC6A was trapped in the nucleus under these conditions (upper panel), the NLS mutated variant was only partially nuclear (middle panel). These observations support our model that the reported NLS is not sufficient for TNRC6 import and so far unidentified Imp $\beta$  contacts might exist. Taken together, we found that Imp $\beta$  facilitates transport of TNRC6 proteins into the nucleus presu-

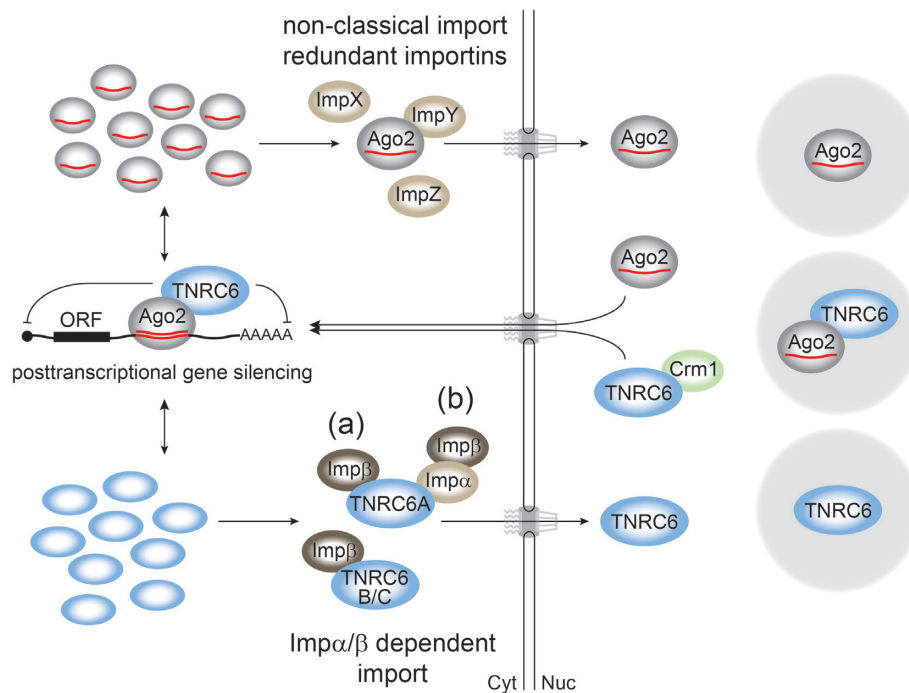


**Figure 8.** A model for nuclear transport of Argonaute and TNRC6 proteins. In the cytoplasm, Argonaute and TNRC6 proteins interact during miRNA-guided gene silencing. Free Argonaute and TNRC6 proteins instead can shuttle between the nucleus and cytoplasm, which may contribute to balancing cytoplasmic levels. Nuclear import of TNRC6 proteins is mediated by Imp $\beta$  (a). TNRC6A can additionally be imported via classical Imp $\alpha/\beta$ -mediated import (b). Nuclear import of Ago proteins instead is non-classical, Imp $\beta$ -independent and probably mediated by several redundant import receptors. Nuclear export of both Ago and TNRC6 proteins is mediated by Crm1. In the nucleus, Ago2 and TNRC6 can interact and co-localize, however, functions of these P-body-like nuclear structures are not known.

ably via canonical, Imp $\alpha$ -dependent processes or by direct TNRC6 interactions.

### Cytoplasmic Ago and TNRC6 levels influence nuclear localization

Since TNRC6 and Ago proteins most likely reach the nucleus via different pathways but form a cytoplasmic complex, we next investigated whether Ago and TNRC6 proteins affect each other's nuclear localization. We co-expressed myc-GFP-TNRC6A NES-mut, which is trapped in the nucleus, together with FH-Ago2 (Figure 6A). Strikingly, myc-GFP-TNRC6A NES-mut exclusively localized to the cytoplasm when high levels of Ago2 are present suggesting that the presence of the binding partner retains TNRC6A in the cytoplasm (Figure 6A, third row of images). This cytoplasmic retention appears to depend on small RNA binding of Ago2 since Ago2-Y529E (68) (or Ago2 PAZ9 (69), images not shown), which cannot bind small RNAs, does not retain TNRC6A in the cytoplasm (Figure 6A, fourth row of images). Furthermore, when the Ago binding motif was mutated together with the NES (TNRC6A  $\Delta$ GW-NES-mut), TNRC6A was not retained in the cytoplasm indicating that indeed Ago binding is responsible for cytoplasmic retention (Figure 6A, sixth row of images). Quantification and protein expression levels are shown to the right. Vice versa, when endogenous TNRC6A, B and C are knocked down simultaneously by a potent siPool (62), nuclear Ago2 levels increase presumably due to a lack of the interaction partner for silencing in the cyto-

plasm (Figure 6B, middle part, upper row). Knock down of individual TNRC6 proteins had no effect on Ago2 localization suggesting redundant TNRC6 protein function (Figure 6B, left part). Signal quantification is shown to the right.

Since Ago expression affects nuclear import of TNRC6A, we asked whether Imp $\alpha/\beta$  and Ago2 binding are mutually exclusive. To test this hypothesis, GST-Imp $\beta$  was immobilized and incubated with radiolabeled TNRC6A (Figure 7A). Indeed, addition of recombinant Ago2 strongly reduced binding to TNRC6A suggesting that the binding partners exclude each other. Similar results were obtained when Imp $\alpha$  isoforms were analyzed (Figure 7B). To exclude binding of recombinant Ago2 to Imp $\alpha$  or  $\beta$  in these assays, we performed direct Ago2 binding experiments (Figure 7C). HA-Ago2 bound specifically to a TNRC6B peptide containing the Ago interacting motif (TNRC6B 599–683) (11). However, binding to Imp $\alpha$  or  $\beta$  was not observed indicating binding to TNRC6 and not the import receptors in our experiments (Figure 7A and B). Since Imp $\beta$  binding is independent of the investigated NLS, another NLS that is affected by Ago binding is most likely present on TNRC6A and the other TNRC6 proteins. To further support our *in vitro* findings, we performed co-immunoprecipitation experiments as described above (Figure 5E). FH-Imp $\beta$  was co-immunoprecipitated with myc-GFP-TNRC6A. However, co-expression of GFP-Ago2 inhibited binding of Imp $\beta$  to TNRC6A. Consistent with our localization studies (Figure 6A), co-expression of the miRNA-binding deficient mutant GFP-Ago2 Y529E did not compete with Imp $\beta$  bind-

ing. Taken together, we have shown that both Ago2 and TNRC6 proteins can influence each other's nuclear levels depending on the availability of the respective binding partner in the cytoplasm.

## DISCUSSION

Mammalian Ago proteins have been implicated in various nuclear functions ranging from transcriptional silencing and activation to DNA double strand break repair and alternative splicing. However, their nuclear import pathways remain elusive. In addition, nuclear localization of other cytoplasmic gene silencing factors has only poorly been investigated (5). Using several different methods, we show that human Ago2 is indeed found in the nucleus. This has been observed in a variety of publications before (46,48,70–71). However, our analyses also suggest that only a minor portion of Ago2 might be present in the nucleus under steady state conditions. It is nevertheless possible that larger portions of the Ago2 pool localize to the nucleus under conditions that have not been analyzed here. For example, it has been reported that Ago2 proteins are found in the nucleus upon senescence induction (70). Using LMB treatment, which blocks Crm1-mediated export, we show that the nuclear pool of Ago2 increases suggesting that at least a part of the Ago pool shuttles between the nucleus and the cytoplasm. It is also conceivable, however, that Ago proteins use additional export routes, which we have not included in our analyses (72). Shuttling also requires nuclear import. The import receptor Imp8 has been implicated in the cytoplasmic function of miRNAs and it was reported that it might also contribute to nuclear localization of mature miRNAs and Ago proteins (50,51). However, by targeting a nuclear RNA (7SK) (47), we find that knock down of Imp8 did not change Ago2-mediated cleavage of the nuclear target. Additionally, none of the other tested import receptors resulted in a change of nuclear RNAi efficiency and therefore we suggest that these proteins might function redundantly and several import receptors are capable of importing Ago proteins into the nucleus. Such redundant transport pathways have been found for several other nuclear factors before including mammalian Dicer (60,63).

Similarly to Ago proteins, TNRC6 proteins localize predominantly to the cytoplasm under steady state conditions. Using LMB treatment, all three TNRC6 proteins are trapped in the nucleus suggesting shuttling and Crm1-mediated export. This has been observed for TNRC6A and B before (17,49). A recent report identified a NES on TNRC6A and mutation of this signal sequence trapped TNRC6A in the nucleus (49). Interestingly, over expressed TNRC6A NES-mut forms P-body-like structures in the nucleus. We characterized these structures further and found that they do not resemble known nuclear structures (Supplementary Figure S2). Also cytoplasmic P-body markers are not recruited to these nuclear TNRC6 bodies. Only, a minor portion of the nuclear Ago2 pool is occasionally found in these structures. We therefore speculate that TNRC6 proteins are capable of forming P-bodies independently of any other cytoplasmic P-body component. This also suggests that TNRC6 proteins might be scaffold proteins within P-bodies probably forming a meshwork by

stacking interactions of the many GW pairs in their large unstructured N-termini. A similar concept has been reported for FG repeats in nucleoporins, which form a meshwork in the nuclear pore (73). However, this needs to be further investigated.

We took advantage of the nuclear localization of the TNRC6A NES-mut and found that Imp $\beta$  targets TNRC6A into the nucleus. This import receptor does not affect Ago nuclear localization indicating that both protein families reach the nucleus via different pathways and are not co-imported (Figure 7). During canonical nuclear import, Imp $\alpha$  binds directly to an NLS and is then bound by Imp $\beta$ , which facilitates nuclear import (64). We find that Imp $\alpha$  binds to a previously identified NLS on TNRC6A. Additionally, Imp $\beta$  contacts TNRC6A independently of Imp $\alpha$  suggesting an Imp $\alpha$ -dependent and -independent import route. TNRC6B and C do not bind to Imp $\alpha$  and are most likely imported by Imp $\beta$  alone.

Interestingly, when over expressing Ago2 in the cytoplasm, even the TNRC6A NESmut version remains in the cytoplasm suggesting that TNRC6 proteins travel through the nucleus in case they are not needed for silencing in the cytoplasm. Consistently, nuclear Ago pools increase, when all three TNRC6 proteins are knocked down suggesting that Ago proteins might be able to shift into the nucleus potentially for storage or turn over. It is tempting to speculate that nuclear import contributes to balanced cytoplasmic Ago2 and TNRC6 protein levels (Figure 8). In contrast, we also observed that TNRC6 mutants, which cannot bind Ago proteins, are still cytoplasmic (data not shown) suggesting that not all unbound TNRC6 proteins are immediately imported into the nucleus. Likewise, so far unknown regulatory processes might exist that trigger TNRC6 or Ago import. For example, post-translational modifications might be involved in such regulatory events. This, however, remains to be investigated.

It is also conceivable that both TNRC6 and Ago proteins possess gene silencing-independent functions in the nucleus of human cells. In future work, it will be interesting to analyze which proteins and RNAs associate with the nuclear TNRC6 protein pool.

## SUPPLEMENTARY DATA

Supplementary Data are available at NAR Online.

## ACKNOWLEDGEMENTS

We thank Sigrun Ammon and Corinna Friederich for technical assistance; Mathias Stotz for HA-Ago2 purification; Kumiko Ui-Tei for plasmids; Laura Corbo, Dirk Eick, Attila Nemeth, David Bentley for antibodies and reagents; Ulrike Kutay and Enno Hartmann for discussions.

*Author contributions:* D.S. performed experiments. S.G.S. and R.D. contributed in vitro binding assays. D.S., J.D., J.P. and E.K. generated and validated monoclonal antibodies. D.S., R.D. and G.M. designed experiments and analyzed data. G.M. and D.S. wrote the manuscript.

## FUNDING

Deutsche Forschungsgemeinschaft [SFB 960, FOR2127]; European Research Council (ERC) [242792 'sRNAs', ITN RNATrain]; Bavarian Genome Research Network (BayGene); Bavarian Systems-Biology Network (BioSysNet). Funding for open access charge: University of Regensburg Deutsche Forschungsgemeinschaft (DFG).

*Conflict of interest statement.* G.M. and S.H. are founders of siTools Biotech, Martinsried, Germany. All other authors declare no conflict of interest.

## REFERENCES

- Meister, G. (2013) Argonaute proteins: functional insights and emerging roles. *Nat. Rev. Genet.*, **14**, 447–459.
- Kuhn, C.D. and Joshua-Tor, L. (2013) Eukaryotic Argonautes come into focus. *Trends Biochem. Sci.*, **38**, 263–271.
- Guang, S., Bochner, A.F., Pavelec, D.M., Burkhart, K.B., Harding, S., Lachowicz, J. and Kennedy, S. (2008) An Argonaute transports siRNAs from the cytoplasm to the nucleus. *Science*, **321**, 537–541.
- Yigit, E., Batista, P.J., Bei, Y., Pang, K.M., Chen, C.C., Tolia, N.H., Joshua-Tor, L., Mitani, S., Simard, M.J. and Mello, C.C. (2006) Analysis of the *C. elegans* Argonaute family reveals that distinct Argonautes act sequentially during RNAi. *Cell*, **127**, 747–757.
- Schraivogel, D. and Meister, G. (2014) Import routes and nuclear functions of Argonaute and other small RNA-silencing proteins. *Trends Biochem. Sci.*, **39**, 420–431.
- Siomi, M.C., Sato, K., Pezic, D. and Aravin, A.A. (2011) PIWI-interacting small RNAs: the vanguard of genome defence. *Nat. Rev. Mol. Cell Biol.*, **12**, 246–258.
- Hutvagner, G. and Simard, M.J. (2008) Argonaute proteins: key players in RNA silencing. *Nat. Rev. Mol. Cell Biol.*, **9**, 22–32.
- Kim, V.N., Han, J. and Siomi, M.C. (2009) Biogenesis of small RNAs in animals. *Nat. Rev. Mol. Cell Biol.*, **10**, 126–139.
- Dueck, A. and Meister, G. (2014) Assembly and function of small RNA – Argonaute protein complexes. *Biol. Chem.*, **395**, 611–629.
- Krol, J., Loedige, I. and Filipowicz, W. (2010) The widespread regulation of microRNA biogenesis, function and decay. *Nat. Rev. Genet.*, **11**, 597–610.
- Pfaff, J., Hennig, J., Herzog, F., Aebersold, R., Sattler, M., Niessing, D. and Meister, G. (2013) Structural features of Argonaute-GW182 protein interactions. *Proc. Natl. Acad. Sci. U.S.A.*, **110**, E3770–E3779.
- Eulalio, A., Huntzinger, E. and Izaurralde, E. (2008) GW182 interaction with Argonaute is essential for miRNA-mediated translational repression and mRNA decay. *Nat. Struct. Mol. Biol.*, **15**, 346–353.
- Chekulaeva, M., Parker, R. and Filipowicz, W. (2010) The GW/WG repeats of *Drosophila* GW182 function as effector motifs for miRNA-mediated repression. *Nucleic Acids Res.*, **38**, 6673–6683.
- Baillat, D. and Shiekhattar, R. (2009) Functional dissection of the human TNRC6 (GW182-related) family of proteins. *Mol. Cell Biol.*, **29**, 4144–4155.
- Takimoto, K., Wakiyama, M. and Yokoyama, S. (2009) Mammalian GW182 contains multiple Argonaute-binding sites and functions in microRNA-mediated translational repression. *RNA*, **15**, 1078–1089.
- Lian, S.L., Li, S., Abadal, G.X., Pauley, B.A., Fritzier, M.J. and Chan, E.K. (2009) The C-terminal half of human Ago2 binds to multiple GW-rich regions of GW182 and requires GW182 to mediate silencing. *RNA*, **15**, 804–813.
- Till, S., Lejeune, E., Thermann, R., Bortfeld, M., Hothorn, M., Enderle, D., Heinrich, C., Hentze, M.W. and Ladurner, A.G. (2007) A conserved motif in Argonaute-interacting proteins mediates functional interactions through the Argonaute PIWI domain. *Nat. Struct. Mol. Biol.*, **14**, 897–903.
- Huntzinger, E. and Izaurralde, E. (2011) Gene silencing by microRNAs: contributions of translational repression and mRNA decay. *Nat. Rev. Genet.*, **12**, 99–110.
- Mathys, H., Basquin, J., Ozgur, S., Czarnocki-Cieciura, M., Bonneau, F., Aartse, A., Dziembowski, A., Nowotny, M., Conti, E. and Filipowicz, W. (2014) Structural and biochemical insights to the role of the CCR4-NOT complex and DDX6 ATPase in microRNA repression. *Mol. Cell*, **54**, 751–765.
- Chen, Y., Boland, A., Kuzuoglu-Ozturk, D., Bawankar, P., Loh, B., Chang, C.T., Weichenrieder, O. and Izaurralde, E. (2014) A DDX6-CNOT1 complex and W-binding pockets in CNOT9 reveal direct links between miRNA target recognition and silencing. *Mol. Cell*, **54**, 737–750.
- Djuranovic, S., Nahvi, A. and Green, R. (2012) miRNA-mediated gene silencing by translational repression followed by mRNA deadenylation and decay. *Science*, **336**, 237–240.
- Bazzini, A.A., Lee, M.T. and Giraldez, A.J. (2012) Ribosome profiling shows that miR-430 reduces translation before causing mRNA decay in zebrafish. *Science*, **336**, 233–237.
- Bethune, J., Artus-Revel, C.G. and Filipowicz, W. (2012) Kinetic analysis reveals successive steps leading to miRNA-mediated silencing in mammalian cells. *EMBO Rep.*, **13**, 716–723.
- Schirle, N.T., Sheu-Gruttadauria, J. and MacRae, I.J. (2014) Gene regulation. Structural basis for microRNA targeting. *Science*, **346**, 608–613.
- Hauptmann, J., Dueck, A., Harlander, S., Pfaff, J., Merkl, R. and Meister, G. (2013) Turning catalytically inactive human Argonaute proteins into active slicer enzymes. *Nat. Struct. Mol. Biol.*, **20**, 814–817.
- Schurmann, N., Trabuco, L.G., Bender, C., Russell, R.B. and Grimm, D. (2013) Molecular dissection of human Argonaute proteins by DNA shuffling. *Nat. Struct. Mol. Biol.*, **20**, 818–826.
- Nakanishi, K., Ascano, M., Gogakos, T., Ishibe-Murakami, S., Serganov, A.A., Briskin, D., Morozov, P., Tuschl, T. and Patel, D.J. (2013) Eukaryote-specific insertion elements control human ARGONAUTE slicer activity. *Cell Rep.*, **3**, 1893–1900.
- Faehnle, C.R., Elkayam, E., Haase, A.D., Hannon, G.J. and Joshua-Tor, L. (2013) The making of a slicer: activation of human Argonaute-1. *Cell Rep.*, **3**, 1901–1909.
- Ma, J.B., Ye, K. and Patel, D.J. (2004) Structural basis for overhang-specific small interfering RNA recognition by the PAZ domain. *Nature*, **429**, 318–322.
- Ma, J.B., Yuan, Y.R., Meister, G., Pei, Y., Tuschl, T. and Patel, D.J. (2005) Structural basis for 5'-end-specific recognition of guide RNA by the *A. fulgidus* Piwi protein. *Nature*, **434**, 666–670.
- Parker, J.S., Roe, S.M. and Barford, D. (2005) Structural insights into mRNA recognition from a PIWI domain-siRNA guide complex. *Nature*, **434**, 663–666.
- Song, J.J., Liu, J., Tolia, N.H., Schneiderman, J., Smith, S.K., Martienssen, R.A., Hannon, G.J. and Joshua-Tor, L. (2003) The crystal structure of the Argonaute2 PAZ domain reveals an RNA binding motif in RNAi effector complexes. *Nat. Struct. Mol. Biol.*, **10**, 1026–1032.
- Yan, K.S., Yan, S., Farooq, A., Han, A., Zeng, L. and Zhou, M.M. (2003) Structure and conserved RNA binding of the PAZ domain. *Nature*, **426**, 468–474.
- Lingel, A., Simon, B., Izaurralde, E. and Sattler, M. (2003) Structure and nucleic-acid binding of the *Drosophila* Argonaute 2 PAZ domain. *Nature*, **426**, 465–469.
- Nakanishi, K., Weinberg, D.E., Bartel, D.P. and Patel, D.J. (2012) Structure of yeast Argonaute with guide RNA. *Nature*, **486**, 368–374.
- Song, J.J., Smith, S.K., Hannon, G.J. and Joshua-Tor, L. (2004) Crystal structure of Argonaute and its implications for RISC slicer activity. *Science*, **305**, 1434–1437.
- Yuan, Y.R., Pei, Y., Ma, J.B., Kuryavyi, V., Zhadina, M., Meister, G., Chen, H.Y., Dauter, Z., Tuschl, T. and Patel, D.J. (2005) Crystal structure of *A. aeolicus* Argonaute, a site-specific DNA-guided endoribonuclease, provides insights into RISC-mediated mRNA cleavage. *Mol. Cell*, **19**, 405–419.
- Liu, J., Carmell, M.A., Rivas, F.V., Marsden, C.G., Thomson, J.M., Song, J.J., Hammond, S.M., Joshua-Tor, L. and Hannon, G.J. (2004) Argonaute2 is the catalytic engine of mammalian RNAi. *Science*, **305**, 1437–1441.
- Meister, G., Landthaler, M., Patkaniowska, A., Dorsett, Y., Teng, G. and Tuschl, T. (2004) Human Argonaute2 mediates RNA cleavage targeted by miRNAs and siRNAs. *Mol. Cell*, **15**, 185–197.
- Petri, S., Dueck, A., Lehmann, G., Putz, N., Rudel, S., Kremmer, E. and Meister, G. (2011) Increased siRNA duplex stability correlates with reduced off-target and elevated on-target effects. *RNA*, **17**, 737–749.
- Wang, D., Zhang, Z., O'Loughlin, E., Lee, T., Houel, S., O'Carroll, D., Tarakhovskiy, A., Ahn, N.G. and Yi, R. (2012) Quantitative functions

- of Argonaute proteins in mammalian development. *Genes Dev.*, **26**, 693–704.
42. Castel, S.E. and Martienssen, R.A. (2013) RNA interference in the nucleus: roles for small RNAs in transcription, epigenetics and beyond. *Nat. Rev. Genet.*, **14**, 100–112.
  43. Janowski, B.A., Huffman, K.E., Schwartz, J.C., Ram, R., Nordsell, R., Shames, D.S., Minna, J.D. and Corey, D.R. (2006) Involvement of AGO1 and AGO2 in mammalian transcriptional silencing. *Nat. Struct. Mol. Biol.*, **13**, 787–792.
  44. Janowski, B.A., Younger, S.T., Hardy, D.B., Ram, R., Huffman, K.E. and Corey, D.R. (2007) Activating gene expression in mammalian cells with promoter-targeted duplex RNAs. *Nat. Chem. Biol.*, **3**, 166–173.
  45. Chu, Y., Yue, X., Younger, S.T., Janowski, B.A. and Corey, D.R. (2010) Involvement of argonaute proteins in gene silencing and activation by RNAs complementary to a non-coding transcript at the progesterone receptor promoter. *Nucleic Acids Res.*, **38**, 7736–7748.
  46. Gagnon, K.T., Li, L., Chu, Y., Janowski, B.A. and Corey, D.R. (2014) RNAi factors are present and active in human cell nuclei. *Cell Rep.*, **6**, 211–221.
  47. Robb, G.B., Brown, K.M., Khurana, J. and Rana, T.M. (2005) Specific and potent RNAi in the nucleus of human cells. *Nat. Struct. Mol. Biol.*, **12**, 133–137.
  48. Rudel, S., Flatley, A., Weinmann, L., Kremmer, E. and Meister, G. (2008) A multifunctional human Argonaute2-specific monoclonal antibody. *RNA*, **14**, 1244–1253.
  49. Nishi, K., Nishi, A., Nagasawa, T. and Ui-Tei, K. (2013) Human TNRC6A is an Argonaute-navigator protein for microRNA-mediated gene silencing in the nucleus. *RNA*, **19**, 17–35.
  50. Weinmann, L., Hock, J., Ivacevic, T., Ohrt, T., Mutze, J., Schwille, P., Kremmer, E., Benes, V., Urlaub, H. and Meister, G. (2009) Importin 8 is a gene silencing factor that targets argonaute proteins to distinct mRNAs. *Cell*, **136**, 496–507.
  51. Wei, Y., Li, L., Wang, D., Zhang, C.Y. and Zen, K. (2014) Importin 8 regulates the transport of mature microRNAs into the cell nucleus. *J. Biol. Chem.*, **289**, 10270–10275.
  52. Kretz, M., Siprashvili, Z., Chu, C., Webster, D.E., Zehnder, A., Qu, K., Lee, C.S., Flockhart, R.J., Groff, A.F., Chow, J. *et al.* (2013) Control of somatic tissue differentiation by the long non-coding RNA TINCR. *Nature*, **493**, 231–235.
  53. Carpenter, A.E., Jones, T.R., Lamprecht, M.R., Clarke, C., Kang, I.H., Friman, O., Guertin, D.A., Chang, J.H., Lindquist, R.A., Moffat, J. *et al.* (2006) CellProfiler: image analysis software for identifying and quantifying cell phenotypes. *Genome Biol.*, **7**, R100.
  54. Steinhoff, A., Pientka, F.K., Mockel, S., Kettelhake, A., Hartmann, E., Kohler, M. and Depping, R. (2009) Cellular oxygen sensing: Importins and exportins are mediators of intracellular localisation of prolyl-4-hydroxylases PHD1 and PHD2. *Biochem. Biophys. Res. Commun.*, **387**, 705–711.
  55. Beitzinger, M., Peters, L., Zhu, J.Y., Kremmer, E. and Meister, G. (2007) Identification of human microRNA targets from isolated Argonaute protein complexes. *RNA Biol.*, **4**, 76–84.
  56. Chapat, C., Kolytcheff, C., Le Romancer, M., Auboeuf, D., De La Grange, P., Chettab, K., Sentis, S. and Corbo, L. (2013) hCAF1/CNOT7 regulates interferon signalling by targeting STAT1. *EMBO J.*, **32**, 688–700.
  57. Brannan, K., Kim, H., Erickson, B., Glover-Cutter, K., Kim, S., Fong, N., Kiemele, L., Hansen, K., Davis, R., Lykke-Andersen, J. *et al.* (2012) mRNA decapping factors and the exonuclease Xrn2 function in widespread premature termination of RNA polymerase II transcription. *Mol. Cell*, **46**, 311–324.
  58. Kudo, N., Wolff, B., Sekimoto, T., Schreiner, E.P., Yoneda, Y., Yanagida, M., Horinouchi, S. and Yoshida, M. (1998) Leptomycin B inhibition of signal-mediated nuclear export by direct binding to CRM1. *Exp. Cell Res.*, **242**, 540–547.
  59. Peterlin, B.M., Brogie, J.E. and Price, D.H. (2012) 7SK snRNA: a noncoding RNA that plays a major role in regulating eukaryotic transcription. *Wiley Interdiscip. Rev. RNA*, **3**, 92–103.
  60. Doyle, M., Badertscher, L., Jaskiewicz, L., Guttinger, S., Jurado, S., Huguenschmidt, T., Kutay, U. and Filipowicz, W. (2013) The double-stranded RNA binding domain of human Dicer functions as a nuclear localization signal. *RNA*, **19**, 1238–1252.
  61. Eulalio, A., Behm-Ansmant, I. and Izaurralde, E. (2007) P bodies: at the crossroads of post-transcriptional pathways. *Nat. Rev. Mol. Cell Biol.*, **8**, 9–22.
  62. Hannus, M., Beitzinger, M., Engelmann, J.C., Weickert, M.T., Spang, R., Hannus, S. and Meister, G. (2014) siPools: highly complex but accurately defined siRNA pools eliminate off-target effects. *Nucleic Acids Res.*, **42**, 8049–8061.
  63. Jakel, S. and Gorlich, D. (1998) Importin beta, transportin, RanBP5 and RanBP7 mediate nuclear import of ribosomal proteins in mammalian cells. *EMBO J.*, **17**, 4491–4502.
  64. Gorlich, D. and Kutay, U. (1999) Transport between the cell nucleus and the cytoplasm. *Annu. Rev. Cell Dev. Biol.*, **15**, 607–660.
  65. Fanara, P., Hodel, M.R., Corbett, A.H. and Hodel, A.E. (2000) Quantitative analysis of nuclear localization signal (NLS)-importin alpha interaction through fluorescence depolarization. Evidence for auto-inhibitory regulation of NLS binding. *J. Biol. Chem.*, **275**, 21218–21223.
  66. Kobe, B. (1999) Autoinhibition by an internal nuclear localization signal revealed by the crystal structure of mammalian importin alpha. *Nat. Struct. Biol.*, **6**, 388–397.
  67. Bischoff, F.R., Klebe, C., Kretschmer, J., Wittinghofer, A. and Ponstingl, H. (1994) RanGAP1 induces GTPase activity of nuclear Ras-related Ran. *Proc. Natl. Acad. Sci. U.S.A.*, **91**, 2587–2591.
  68. Rüdell, S., Wang, Y., Lenobel, R., Körner, R., Hsiao, H., Urlaub, H., Patel, D. and Meister, D. (2011) Phosphorylation of human Argonaute proteins affects small RNA binding. *Nucleic Acids Res.*, **39**, 2330–2343.
  69. Liu, J., Valencia-Sanchez, M.A., Hannon, G.J. and Parker, R. (2005) MicroRNA-dependent localization of targeted mRNAs to mammalian P-bodies. *Nat. Cell Biol.*, **7**, 719–723.
  70. Benhamed, M., Herbig, U., Ye, T., Dejean, A. and Bischof, O. (2012) Senescence is an endogenous trigger for microRNA-directed transcriptional gene silencing in human cells. *Nat. Cell Biol.*, **14**, 266–275.
  71. Gagnon, K.T. and Corey, D.R. (2012) Argonaute and the nuclear RNAs: new pathways for RNA-mediated control of gene expression. *Nucleic Acids Therap.*, **22**, 3–16.
  72. Guttler, T. and Gorlich, D. (2011) Ran-dependent nuclear export mediators: a structural perspective. *EMBO J.*, **30**, 3457–3474.
  73. Labokha, A.A., Gradmann, S., Frey, S., Hulsmann, B.B., Urlaub, H., Baldus, M. and Gorlich, D. (2013) Systematic analysis of barrier-forming FG hydrogels from Xenopus nuclear pore complexes. *EMBO J.*, **32**, 204–218.